Malaysian Journal of Analytical Sciences
(MJAS)
Published by Malaysian Analytical Sciences Society
ANALIS
Persatuan Sains Analisis Malaysia

SODIUM ALGINATE/β-CYCLODEXTRIN AS SUPRAMOLECULAR HYDROGEL FOR ADSORPTION OF PERFLUOROOCTANE SULFONATE

(Natrium Alginat/β-Siklodekstrin Sebagai Hidrogel Supramolekul untuk Penjerapan Perfluorooktana Sulfonat)

Aiza Farhani Zakaria[1], Norizah Abdul Rahman[1], Noorfatimah Yahaya[3], Wan Nazihah Wan Ibrahim[4],
Saw Hong Loh[5], Dyia Syaleyana Md Shukri[6] and Sazlinda Kamaruzaman[1,2*]

[1]*Department of Chemistry, Faculty of Science, Universiti Putra Malaysia, 43400, UPM Serdang Selangor, Malaysia*
[2]*Natural Medicines and Product Research Laboratory (NaturMeds), Institute of Bioscience (IBS), Universiti Putra Malaysia, 43400, UPM Serdang Selangor, Malaysia*
[3]*Integrative Medicine Cluster, Advanced Medical and Dental Institute, Universiti Sains Malaysia, 13200 Kepala Batas, Penang, Malaysia*
[4]*Faculty of Applied Sciences, Universiti Teknologi MARA, 40450 Shah Alam, Selangor, Malaysia*
[5]*Faculty of Science and Marine Environment, Universiti Malaysia Terengganu, 21030 Kuala Nerus, Terengganu, Malaysia*
[6]*Faculty Applied Sciences, Universiti Teknologi MARA Cawangan Perlis, Kampus Arau, 02600 Arau, Perlis.*

Corresponding author: sazlinda@upm.edu.my

Received: 1 September 2023; Accepted: 24 July 2024; Published: 27 October 2024

Abstract

Perfluorooctane sulfonate (PFOS) has been classified as a persistent organic pollutant that contributes to water pollution due to its slow environmental degradation properties. Due to the need for effective removal of PFOS from polluted water bodies, a supramolecular hydrogel incorporating sodium alginate and β-cyclodextrin (SA-β-CD hydrogel) was developed to facilitate the entrapment of PFOS. The adsorption study has been utilised to remove PFOS via batch experiment procedure on several adsorptive parameters such as pH, contact time and initial concentration. The optimum conditions with a dose of 1280 mg of SA-β-CD hydrogels beads were applied at 70°C, contact time of 30 minutes, pH of 5.5, 10 mL of 10.0 ppm of PFOS solution, and 250 rpm of stirring rate were reported. The adsorption capacity and efficiency removal of PFOS by SA-β-CD hydrogel beads has achieved up to 0.0764 mg/g and 84.72%, respectively. Based on the data obtained, the adsorption kinetic study, which follows a pseudo-second-order model, was fitted to illustrate the adsorption of PFOS by SA-β-CD hydrogel beads, with an R^2 value of 0.990. The adsorption isotherm study showed that the adsorption of PFOS by SA-β-CD hydrogel beads fits the Langmuir isotherm model, with an R^2 value of 0.987. The adsorption of PFOS occurs as a monolayer/single layer and involves chemisorption to the hydrogel beads. Therefore, this work demonstrates that SA-β-CD hydrogel beads may be useful in controlling environmental water pollution.

Keywords: water pollution, persistent organic pollutant, perfluorooctane sulfonate, hydrogel

Abstrak

Perfluorooktana sulfonat (PFOS) telah diklasifikasikan sebagai bahan pencemar organik berterusan yang menyumbang kepada pencemaran air disebabkan oleh sifat degradasi alam sekitar yang perlahan. Oleh sebab itu, hidrogel supramolekul yang menggabungkan natrium alginat dan β-siklodekstrin (hidrogel SA-β-CD) telah dibangunkan untuk membantu memerangkap PFOS daripada badan air yang tercemar. Kajian penjerapan telah digunakan untuk mengeluarkan PFOS melalui prosedur eksperimen kelompok pada beberapa parameter penjerapan seperti pH, masa sentuhan dan kepekatan awal. Keadaan optimum dengan dos 1280 mg manik hidrogel SA-β-CD digunakan pada 70°C, masa sentuhan 30 minit, pH 5.5, 10 mL larutan PFOS 10.0 ppm, dan 250 rpm kadar kacau dilaporkan. Kapasiti penjerapan dan penyingkiran kecekapan PFOS oleh manik hidrogel SA-β-CD telah mencapai sehingga 0.0764 mg/g dan 84.72%, masing-masing. Berdasarkan data yang diperoleh, kajian kinetik penjerapan yang merupakan model pseudo-tertib dua telah digunakan untuk menggambarkan penjerapan PFOS oleh manik hidrogel SA-β-CD dengan nilai R^2 yang diperolehi ialah 0.990. Manakala kajian penjerapan isoterma, penjerapan PFOS oleh manik hidrogel SA-β-CD telah digunakan pada model Langmuir isoterma dengan nilai R^2 yang diperolehi ialah 0.987. Penjerapan PFOS berlaku sebagai lapisan tunggal/satu lapisan dengan penjerapan kimia kepada manik hidrogel. Oleh itu, kerja ini menunjukkan bahawa manik hidrogel SA-β-CD boleh membantu sebagai inisiatif untuk mengawal pencemaran air di alam sekitar.

Kata kunci: pencemaran air, pencemar organik berterusan, perfluorooktana sulfonat, hidrogel

Introduction

The level of surface water contamination and drinking water by persistent organic pollutants (POPs) has caused an emerging concern worldwide, especially from the scientific community [1,3]. One of the persistent organic pollutants identified in water resources are perfluorinated compounds, which perfluorooctane sulfonate (PFOS) will be highlighted throughout this research work. PFOS was categorised as a persistent organic pollutant in the fourth meeting of the conference at the Stockholm Convention in May 2009, which has been known to contribute to public health problems [3]. According to Zhao et al., PFOS and its precursors have been detected worldwide, especially in water sources, sediments, blood sera, and livers of humans and various wildlife species, and reported as innocuous and harmful to humans and the environment [4]. In the circumstances, the exertion to discover an effective way to remove PFOS from the environment is challenging because it remains in the environment for a long time because of its high chemical and thermal stability, bioaccumulate, persistence, and difficulty to degrade in the natural environment [4,5,6]. Recently, many technologies have been developed to remove PFOS from the water environment, such as adsorption, precipitation, filtration, and photodegradation; however, most of them have several limitations, like slow adsorption efficiency and high cost of treatment [7]. Nevertheless, the adsorption method is recognised to be a prominent technique for minimising the quantity of PFOS from the aqueous environment. This is because it has a simple, practical procedure, low cost, high removal efficiency, and is less toxic, without releasing any secondary contaminants. In this work, a sustainable and green hydrogel adsorbent in bead form was developed and utilised to address water pollution caused by PFOS in the aqueous environment [8,9].

To address the limitations of current adsorbents, a study was conducted to develop cost-effective and environmentally friendly adsorbents using a range of natural raw materials in the form of a hydrogel. Hydrogels are hydrophilic three-dimensional (3D) network polymers that can swell and retain water quantities in their morphology [9,10]. This study focused on developing hydrogel using natural polymer biomaterials as primary constituents. They are driven by their advantages, reliability, capacity to degrade naturally, convenient accessibility, cost-effectiveness in production and regeneration, and overall ecological compatibility. Sodium alginate (SA) is a sodium salt of alginic acid that can be extracted from the cell wall of brown algae. It is commonly used as a chemical substance in hydrogel production due to its low level of toxicity, excellent adsorption ability, and low production cost [10,11]. In recent applications, SA hydrogels have been modified with various organic/inorganic chemicals to increase their adsorption efficiency towards selected pollutants in the water environment. However, in this work, the reinforcement of cyclodextrins (CD) has been expected to improve the mechanical properties of SA [12]. Moreover, CDs are macrocyclic oligosaccharides synthesised as products of starch enzymatic digestion and have a high inclusion ability due to their unique hydrophobic and hydrophilic properties. [13]. There are three types of CDs identified by previous scientists such as α-cyclodextrin (α-CD), β-cyclodextrin (β-CD), and γ-cyclodextrin (γ-CD). Among them, β-CD is the most widely used in the pharmaceutical field for its ability to improve the solubility and the stability of drugs by complex formation at the solid state [14,15]. Qin et al. exclaimed that the properties of β-CD that are hydrophobic that enable to form inclusion complexes of host-guest with numerous types of organic pollutants, and its hydroxyl groups on the hydrophilic edge can be modified according to functional groups to bind with guest compound [16,17]. For that reason, β-CD has been selected in this work to produce supramolecular hydrogel.

In this study, sodium alginate-β-cyclodextrin (SA-β-CD) hydrogel beads were prepared, characterised, and utilised as adsorbents to adsorb the PFOS in the water. The chemical and physical characteristics of the SA-β-CD hydrogels were examined through field emission scanning electron microscopy (FESEM) and Fourier transform infrared (FTIR). In addition, several essential adsorption parameters, such as solution pH, contact time, and initial concentration, were thoroughly studied to determine the adsorption capacity and removal efficiency of the synthesised SA-β-CD hydrogel towards PFOS.

Material and methods

Materials

Sodium alginate biopolymer with viscosity of 300-400 Pa s was purchased from Chemiz (M) Sdn. Bhd. (Selangor, Malaysia). β-cyclodextrin was purchased from Sigma-Aldrich, (Darmstadt, Germany). Calcium chloride was purchased from Progressive Scientific Sdn. Bhd. (Selangor, Malaysia). All other chemical reagents used were of chromatographic or analytical grade or better and were used as received. 0.1 M NaOH and 0.1 M HCl were used to adjust the pH of the solutions. Distilled water was used for the preparation of working standard of PFOS solutions.

SA-β-CD hydrogel preparation

An amount 0.9 g of sodium alginate and 2.8 g of β-cyclodextrin were added into 50 mL deionised water. Then, 100 μL of epichlorohydrin and 10 mL of 0.5 M NaOH solution was slowly added into the solution. The mixture was shaken in a water bath for 3.5 hours at 70°C and the obtained solution was cooled at room temperature. To form the SA-β-CD hydrogel beads, the mixture was extruded into 0.1 M $CaCl_2$ solution with a 20 mm syringe. The hydrogel beads were left undisturbed in the $CaCl_2$ solution for 2 hours to solidify. Next, the hydrogel beads were filtered and washed with a 0.1 M HCl solution. Lastly, some of the prepared gel beads were refrigerated at 4°C for storing purpose and some were dried in the open air.

Characterisations of SA-β-CD hydrogel

SA-β-CD hydrogel was characterised with several high technology instruments. Fourier emission scanning electron microscopy (FESEM, JEOL JSM-7600F) was used to determine the surface morphology of the hydrogel. Fourier transform infrared spectroscopy (FTIR, Perkin Elmer Spectrum RXI Fourier transformed infrared spectrophotometer) was applied to test the functional groups.

PFOS batch adsorption procedure

The adsorption procedure of PFOS on SA-β-CD hydrogel bead were studied in batch mode experiment. The parameters were varied according to the conditions for the experimental study: contact time, pH of the sample and initial concentration of PFOS solution. All experiments are being performed at room temperature by optimising one parameter while keeping the other parameters constant. 10 ml of PFOS solution was placed in a fixed volume conical flask. SA-β-CD hydrogel beads were added to the solution with constant stirring at a constant room temperature and shaken to establish equilibrium. Then the adsorbent was separated through a filter and the equilibrium concentration, Ce, of the PFOS solution was measured using UV-Vis spectrometer. To obtain accurate and precise result of the experiments, the adsorption processes were repeated three times under optimum conditions. The adsorption capacity of PFOS from each adsorption parameter were calculated by using Equation 1. Meanwhile, the percentage of removal of PFOS was calculated using Equation 2.

$$q_e = \left(\frac{C_o - C_e}{m}\right) \text{ x } V \qquad (1)$$

$$\% \text{ removal} = \left(\frac{C_o - C_e}{C_o}\right) \text{ x } 100\% \qquad (2)$$

where q_e is the amount of the PFOS adsorbed at equilibrium, Co is the initial concentration of a PFOS solution, Ce is the final concentration of a PFOS solution, m is the mass of SA-β-CD hydrogel used and V is the volume of the sample solution.

Adsorption isotherm and kinetics

To study the adsorption nature of PFOS onto the SA-β-CD hydrogel, Langmuir and Freundlich isotherm models were adapted. Their expressions are as follows:

$$1/q_e = 1/Q_{max} + 1/bQ_{max} \cdot 1/Ce \qquad (3)$$

where C_e is the liquid-phase concentrations of PFOS at equilibrium express in mg·g^{-1}, q_e is the amount of PFOS adsorbed at equilibrium can be expressed in mg·g^{-1}, Q_{max} is the maximum monolayer adsorption capacity express in mg· g^{-1}, and b is the Langmuir constant express in L· mg^{-1} or L·mol^{-1}. The values of Q_{max} and b were calculated from the slope and intercept of the different straight lines representing to different temperatures [18,19]. Freundlich isotherm expression can be defined as follows:

$$\ln q_e = \ln K_f + (1/n) \ln C_e \qquad (4)$$

where Ce is the liquid-phase concentrations of adsorbate at equilibrium (mg·L^{-1}) and q_e is the amount of solute adsorbed at equilibrium (mg·g^{-1}). K_f and 1/n are Freundlich constants related to capacity of sorption and favourability of sorption, respectively. K_f (mg·g^{-1}) (L·mg^{-1})$^{1/n}$ is the adsorption capacity of the adsorbent and n indicates the degree of favourability of an adsorption process. In addition, the sorption is considered favourable when the value of n in the range of $0 < n < 10$. The greater value of n represents the adsorption process is more favourable [18,20].

To ascertain the adsorption mechanism of PFOS, pseudo-first-order and pseudo-second-order kinetic models were used. The adsorption kinetic study is usually used to identify the adsorption rate and potential rate-controlling of the adsorption mechanism process [21,22]. The experimental adsorption phenomenon ordinarily employed the pseudo-first-order which basically focuses on the difference in equilibrium adsorption capacity as well as adsorbed amount and pseudo-second-order model which considering the assumption of the rate-limiting step involves chemisorption. Correlated to that the pseudo-first-order and pseudo-second-order have been defined as following equation:

$$\ln (q_e - q_t) = \ln q_e - k_t t \qquad (5)$$

$$t/q_t = 1/k_2 q_e^2 + 1/q_e \cdot t \qquad (6)$$

where, q_e (mg·g^{-1}) means equilibrium adsorption capacity, q_t (mg· g^{-1}) the adsorption capacity at t moment, k_1 (min^{-1}) and k_2 (min $^{-1}$) the rate constant for pseudo-first-order kinetic model and pseudo-second order kinetic model respectively [23, 24].

Results and Discussion

The physical characteristics of the prepared SA-β-CD hydrogel beads

Figure 1 shows the visual image of the synthesised SA-β-CD hydrogel beads. It reveals that the physical appearance of the SA-β-CD hydrogel beads was clear in colour, and each hydrogel bead's mass and diameter size were recorded to be approximately 32 mg and 3 mm, respectively. According to existing knowledge, no literature has yet discussed the development of hybrid supramolecular hydrogels by combining natural biopolymers like sodium alginate (SA) and β-cyclodextrin (β-CD). The incorporation of β-CD into the SA polymer matrix aims to improve the hydrogel's properties as an adsorbent, including creating a large porous structure, high surface area, and extensive surface reactivity suitable for water treatment applications. β-CD is favourable for incorporation due to its abundance of hydrogen bond donors, which support the formation of hydrogen bonds with alginate. Additionally, the oxygenated functional groups, such as carboxyl and hydroxyl groups in both alginate and β-CD, interact with each other during the immobilisation technique. In this work, the focus is on developing a smart adsorbent and discussing its adsorption behaviour for removing PFOS from aqueous environmental samples.

Spectroscopic study of SA-β-CD hydrogel beads

Figure 2 (a) and (b) shows FTIR spectra for SA hydrogel and SA-β-CD hydrogel beads, respectively. The stretching of the C-O group produced a large peak in the spectrum of SA at 1030 cm^{-1}. A sharp peak at 1261 cm^{-1} confirmed the presence of the arabinosyl functionality, and sharp peaks at 940 cm^{-1} and 874 cm^{-1} were due to the -glycosidic linkage between the mannuronic and guluronic units in the G, M unit group stretching vibration of SA. The sp^3 C-H asymmetric stretching mode and the C-OH bending vibration were responsible for the large peaks at 2963 cm^{-1} and 1432 cm^{-1}. O-H and C-O-C group stretching vibrations resulted in large peaks at 3394 cm^{-1} and 1027 cm^{-1}. A prominent peak intensity at 1728 cm^{-1} indicated the monomer grafted onto the SA backbone after sodium alginate was polymerised with β-CD. Sharp peaks at 1632 cm^{-1} and 1728 cm^{-1} were attributed to the symmetric and asymmetric COO- group vibrations, respectively. Most of the carboxyl group had been successfully cross-linked with the hydroxyl group of SA and β-CD in the system. Previous papers have shown similar patterns, suggesting that the cross-linking and incorporation processes produced comparable functional group interactions in both hydrogel beads [29-33].

After incorporating β-CD, the leading functional group observed was hydroxyl, with OH stretching strong and broad at 3401 cm^{-1}, indicating successful binding of SA and β-CD. The broadness might also be due to the mixture of O-H groups in both β-CD and SA structures, attributing to the wide and large O-H vibration. A medium peak at 2929 cm-1 was assigned to C-H stretching, and the band at 1720 cm^{-1} was related to C=O. Medium peaks of C-O stretching were observed at 1087 and 1062 cm^{-1}. The peaks at 3401, 1087, and 772 cm^{-1} in the spectrum of SA-β-CD hydrogel beads indicated the presence of β-CD, while peaks at 946 and 864 cm^{-1} are prominent in the SA hydrogel. The peak at 1062 cm^{-1} corresponds to C-O, which might have formed between β-CD and epichlorohydrin, aligning with findings by Shen et al. These similarities suggest that the cross-linking and incorporation processes produced comparable functional group interactions in both hydrogel beads [34-37].

Figure 1. Physical appearance of synthesized SA-β-CD hydrogel beads.

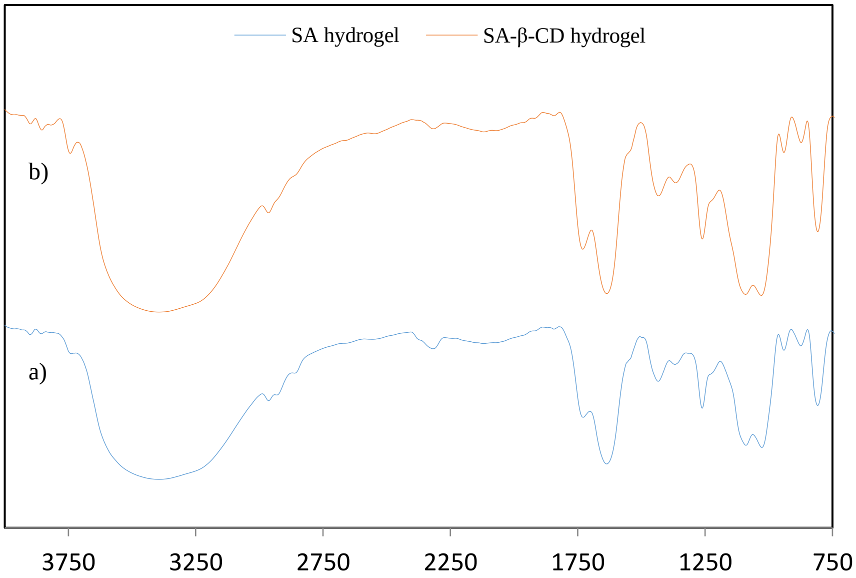

Figure 2. FTIR spectra of (a) SA hydrogel (b) SA-β-CD hydrogel.

Surface morphology of SA-β-CD hydrogel

Figure 3(a) shows the FESEM morphologies of SA-β-CD hydrogel beads before PFOS adsorption, revealing notable surface coverage. The porosities of these beads are clearly visible under different magnifications in Figure 3a (i) and (ii). The FESEM images display a rough and irregular morphology with many wrinkles and non-smooth surfaces, indicating the presence of functional groups on the surface of the SA-β-CD hydrogel. These features suggest that the SA-β-CD hydrogel beads have superior adsorption sites for PFOS penetration. In contrast, Figure 3(b) shows the FESEM morphologies the SA hydrogel beads typically exhibited a smoother surface with fewer irregularities and less pronounced porosity. This difference in surface morphology is significant, as the presence of β-CD in the hydrogel matrix introduces additional functional groups and porosity, enhancing the adsorption capacity and efficiency of the hydrogel beads. The rough and wrinkled surface of the SA-β-CD hydrogel provided more active sites for PFOS binding compared to the smoother surface of the SA hydrogel, making the former a more effective adsorbent for PFOS removal.

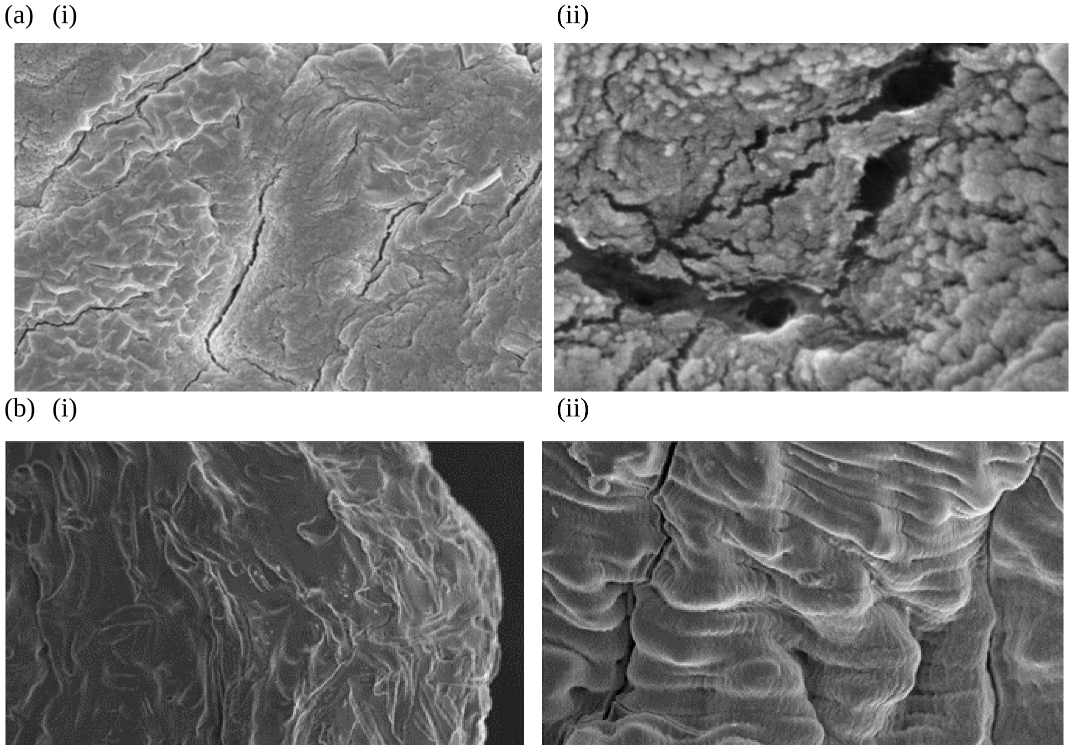

Figure 3. Surface morphologies of (a) SA-β-CD hydrogel beads under magnifications of (i) 2,5000 (ii) 50,000 and (b) SA hydrogel beads under magnifications of (i) 2,5000 (ii) 50,000.

Adsorption experiment of PFOS: Effect of initial concentration

Figure 4 shows the graph that studies the relationship between adsorption capacity and the percentage removal of PFOS at various initial concentrations. The initial concentration of PFOS varied from 0.5 ppm to 10.0 ppm to determine the ability of the adsorbent to capture PFOS. Although the studied concentrations are above the permitted limit (70 ng/L), this approach was chosen to thoroughly test the adsorption capability of the beads. This study served as a preliminary investigation, demonstrating the potential of the beads for PFOS adsorption and providing a basis for further optimisation. Future work can refine the adsorption process to ensure effectiveness at environmentally relevant PFOS concentrations. [39,40]. From Figure 4, the removal uptake of PFOS on SA-β-CD had gradually increased from 0.5 mg/L to 10 mg/L with the maximum adsorption capacity from 0.00079 mg/g to 0.05676 mg/g. Moreover, the highest percentage removal of

PFOS using SA-β-CD hydrogel beads can be observed at 10.0 ppm, where the percentage removal of PFOS reached 72.76%. However, the lowest initial concentration for the elimination of PFOS is when the initial concentration used was 0.5 ppm at 16.67% of removal. These observations could be attributed to the active sites of the adsorbent, which become more accessible to PFOS at higher concentrations [41]. Additionally, the removal efficiency might be due to the high availability of adsorption sites on the SA-β-CD surface. This surface provides additional penetration sites and functional groups, such as oxygen-containing functional groups, including hydroxyl and carbonyl, for PFOS adsorption. As a result, this increases the hydrophobicity, electrostatic interactions, and hydrogen bonding between PFOS and the adsorption surface of the SA-β-CD hydrogel [42, 43]. Consequently, the equilibrium adsorption capacity of SA-β-CD hydrogel beads increased as the initial concentration of PFOS escalated. Hence, 10 ppm of PFOS was used as the optimal initial concentration for further adsorption studies.

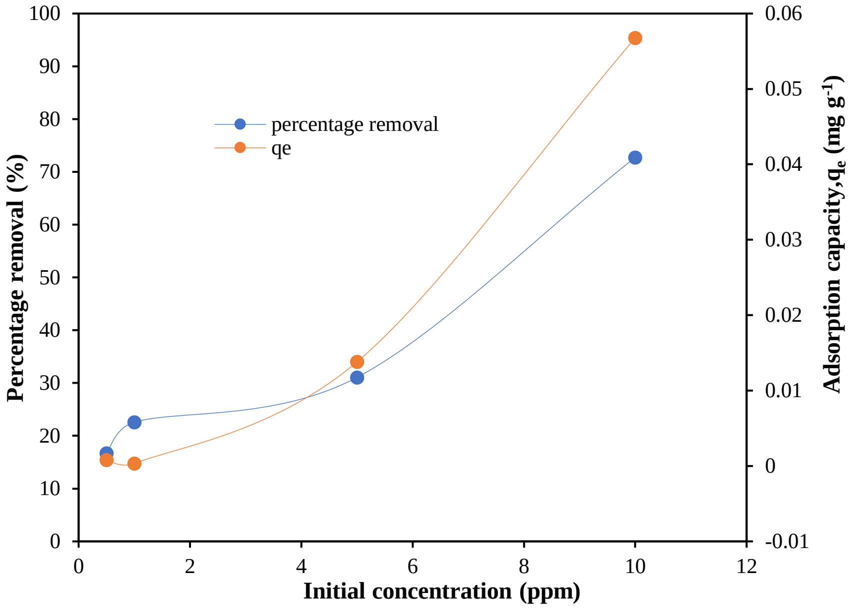

Figure 4. Effect of initial concentration on the percentage removal and adsorption capacity, q_e of PFOS. Adsorption condition: 1280 mg SA-β-CD hydrogel beads in 10 mL of PFOS solution, pH of 3, contact time of 30 minutes, stirring rate of 250 rpm and conducted at room temperature.

Effect of pH

Figure 5 illustrates the effect of the pH of PFOS solution varied from 3 to 8 while others were kept constant. Based on the graph, the elimination of PFOS was shown to be substantially reliant on the pH of the PFOS solution throughout this study. The percentage removal and the adsorption capacity of PFOS using SA-β-CD hydrogel beads decreased as the pH value increased. The result shows that since the adsorption of PFOS is pH dependent, the removal efficiency of PFOS by SA-β-CD hydrogel influenced the adsorption to be most favourable to achieve at lower pH compared to higher pH [44]. In comparison, adsorbent-analyte interaction decreases at higher pH, resulting in a lower percentage of PFOS removal. These explanations can be seen in Figure 5, where at pH 3, the percentage removal of PFOS was the highest at 39.47%, while at pH 8, the percentage removal of PFOS was the lowest at 24.55% [45]. This may be because the acid dissociation constant (pKa) for PFOS was -3.27. Since PFOS's pKa value is less than 1, it mainly resided in the solution as an anion. In the adsorption process of PFOS, electrostatic attraction plays a significant role [46,47].

Thus, in most cases, PFOS exist as anions, while the active binding site of SA-β-CD hydrogel beads used as adsorbents exist as cations. However, adsorbents and analytes will have negatively charged surfaces at a certain high pH (higher than the pKa value of PFOS). This effect causes electrostatic repulsion, which hampers adsorption since the contacts between the analyte and the active binding sites of the adsorbents are weakened under these conditions, making the adsorption process more reversible [48]. Increased pH can result in a minor decrease in PFOS adsorption due to enhanced electrostatic interaction between PFOS and the adsorbents [49]. At pH 5 and 6, the percentage removal of PFOS increased slightly compared to pH 4, as the optimum pH for PFOS adsorption was pH 5.5, before decreasing at pH 7. However, the adsorption capacity at pH 5 to 11 gradually decreased which may be due to the hydroxide ion dominating the hydrogen bonding interaction with the adsorbent [50]. Therefore, the adsorption capacity at pH 3 was used for further study. The determination of the ionisation degree and speciation of the analytes, as well as the surface charge of the adsorbent, were necessitated by pH optimization. Hence, pH 3 has been selected as the optimum pH for the next adsorption investigation.

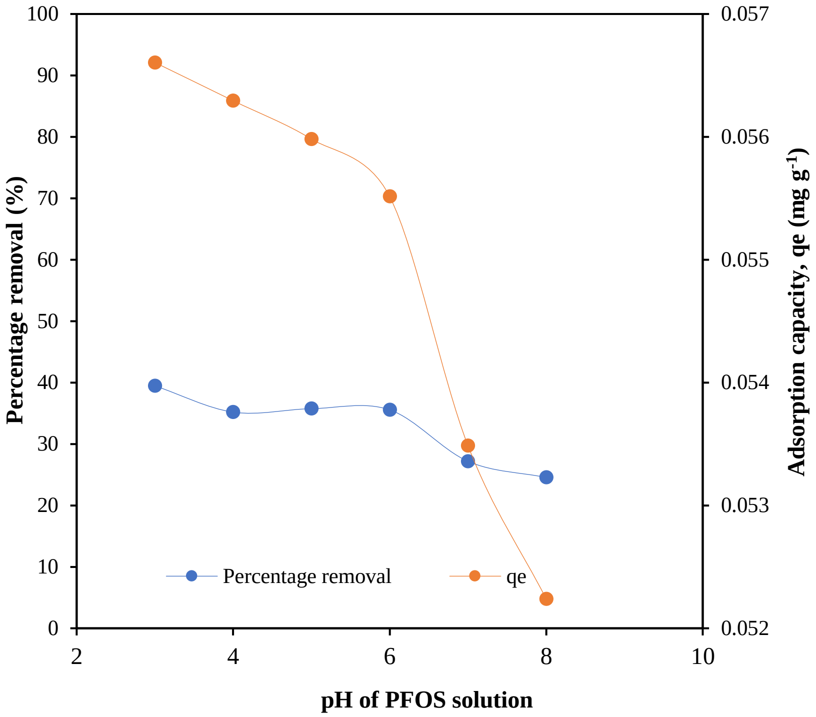

Figure 5. Effect of pH on the percentage removal (%) and adsorption capacity, q_e (mg g^{-1}) of PFOS. Adsorption condition: 1280 mg SA-β-CD hydrogel beads in 10 mL of 10.0 ppm PFOS solution, contact time of 30 minutes, stirring rate of 250 rpm and conducted at room temperature.

Effect of contact time

To predict the adsorbent's efficiency and feasibility in removing PFOS from aqueous solution, the reaction contact time was used as one of the parameters to calculate the efficiency of the SA-β-CD hydrogel beads to remove the PFOS pollutant [51]. This parameter was used to study the relationship between the reaction contact time with the adsorption of the SA-β-CD hydrogel beads for PFOS removal. Figure 6 below shows the relationship between contact time and the percentage of removal and adsorption capacity of PFOS from the aqueous solution. The graph reported that the highest percentage of PFOS removal was at 60 minutes, with 61.81% removal, while the lowest percentage removal of PFOS recorded was at 10 minutes, with 40.64% removal efficiency. The percentage removal of PFOS increased gradually as the contact time with SA-β-CD hydrogel increased, which may be due to the significant number of active binding sites available on the adsorbent. These sites can interact with more PFOS as the contact time increases. The active adsorption sites tend to saturate with PFOS over time [52]. This might be due to the abundance of hydroxyl groups (-OH) on the outer surface of β-CD, which can form hydrogen bonds with PFOS or other functional groups within the hydrogel, enhancing the interaction and adsorption capacity. The formation of hydrogen bonds can increase the effective surface area by providing additional binding sites. Thus, the longer the time for the hydrogel beads to come in contact with PFOS the more interaction of PFOS has with the binding sites, resulting in higher adsorption of PFOS. Hence, the percentage removal of PFOS increased as contact time increased [53].

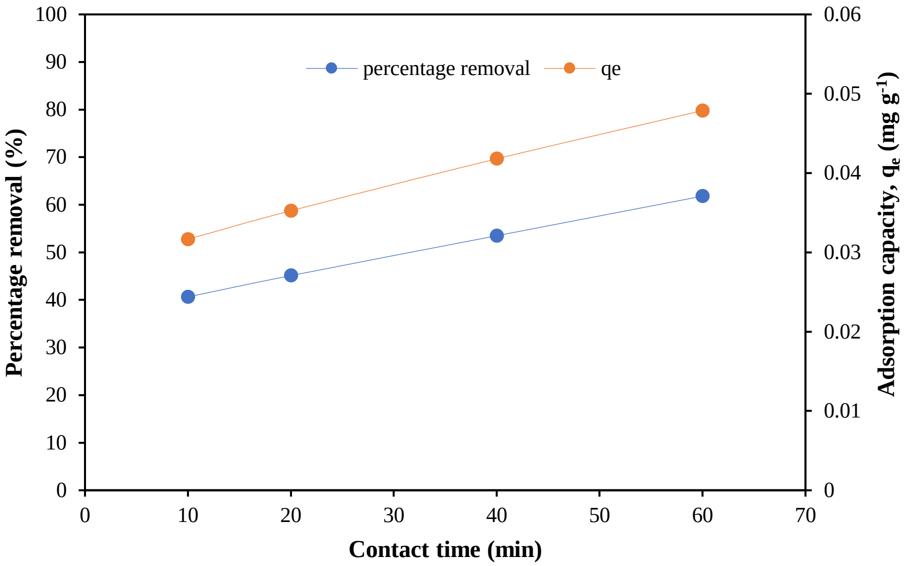

Figure 6. Effect of contact time on the percentage removal and adsorption capacity, q_e of PFOS. Adsorption condition: 1280 mg SA-β-CD hydrogel beads in 10 mL of 10.0 ppm PFOS solution, pH of 3, stirring rate of 250 rpm and conducted at room temperature.

Adsorption isotherm study

Langmuir and Freundlich isotherm models were used to examine the relationship between the quantity of PFOS adsorbed onto SA-β-CD hydrogel beads and its equilibrium concentration in an aqueous environment. Moreover, both models represented the connection between the quantity of PFOS adsorbed by the adsorbent and the final amount of PFOS concentration in the solution once the system reaches equilibrium at a constant temperature. Figure 7 below shows the graph of the Langmuir isotherm model and the Freundlich isotherm model for the adsorption of PFOS. As seen from the adsorption data, the R^2 value obtained for the Langmuir isotherm model was 0.987, while the R^2 value obtained for the Freundlich isotherm model was 0.671. Since R^2 for the Langmuir isotherm is higher than the Freundlich isotherm model, the Langmuir isotherm model was suitable for describing the adsorption study for the PFOS removal experiment [44, 53]. The results suggested that the Langmuir isotherm model is more favourable for the adsorption process of PFOS on the SA-β-CD hydrogel surface that occurred at the monolayer adsorption sites and exhibit a homogenous morphology with a finite number of adsorption sites on SA-β-CD surface [54]. Hence, the findings can be concluded that the experimental data was perfectly suited to the Langmuir isotherm model for the adsorption of PFOS compared to the Freundlich isotherm model, which is in good agreement with the results reported by Elanchezhiyan et al. for the adsorption of PFOS onto the surface magnetic Zr-$MnFe_2O_4$@rGO nanohybrid [55].

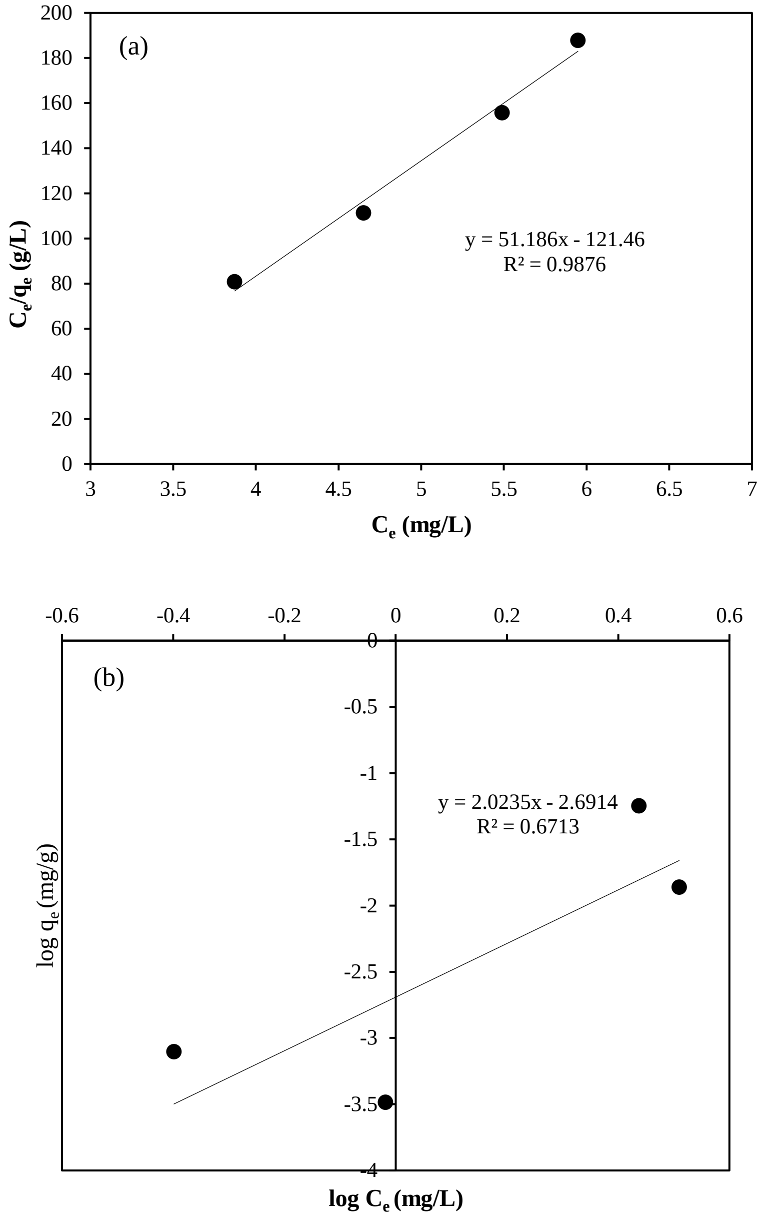

Figure 7. Graph of a) Langmuir isotherm b) Freundlich isotherm model for the adsorption of PFOS

Table 1. Adsorption isotherm parameters

Isotherm	Parameter	
Langmuir	B (L/mg)	-0.421
	q_m (mg/g)	0.019
	R^2	0.987
Freundlich	k	0.002
	n	0.494
	R^2	0.671

Adsorption kinetic study

The adsorption kinetic model was used to explore the adsorption mechanism and potential rate control to determine the rate of PFOS adsorption into the binding site of SA-β-CD hydrogel. Pseudo-first-order and pseudo-second-order were applied as adsorption kinetic models to describe this study's adsorption rate. The pseudo-first-order and pseudo-second-order equations are shown in Equation 5 and Equation 6, respectively [56]. Figure 8 below shows the best-fit line graph of the pseudo-first-order kinetic and pseudo-second-order kinetic for the adsorption of PFOS. Meanwhile, Table 2 lists the adsorption kinetic parameters for both pseudo-first order and pseudo-second order kinetic parameter that includes the obtained R^2 rate constant, (k), and adsorption capacity of PFOS at equilibrium. From the findings for both kinetic models, the R^2 value belonging to the pseudo-first second order had a higher value than the pseudo-first order, which was 0.9900 and 0.9879, respectively. Hence, the results suggested that the pseudo-second-order model was more fitted and suitable to illustrate the adsorption of PFOS on the SA-β-CD hydrogel beads as per the study reported by Guo et al. [44]. The experimental data obtained was fitted and correctly followed the theory as the result showed that it was fitted to pseudo-second pseudo-second-order kinetic model and assumed that chemical sorption or chemisorption is the rate-limiting step for this adsorption study [57-59]. It also helped to predict the behaviour over the whole adsorption range. Hence, it could be concluded that pseudo-second-order is the most suitable to describe the adsorption process.

Table 2. Adsorption kinetic parameters

Kinetic Model	Parameters	
Pseudo-first order	k_1 (1/min)	0.020
	q_e (mg/g)	0.032
	R^2	0.987
Pseudo-second order	k_2 (g/mg min)	2.043
	q_e (mg/g)	0.053
	R^2	0.990

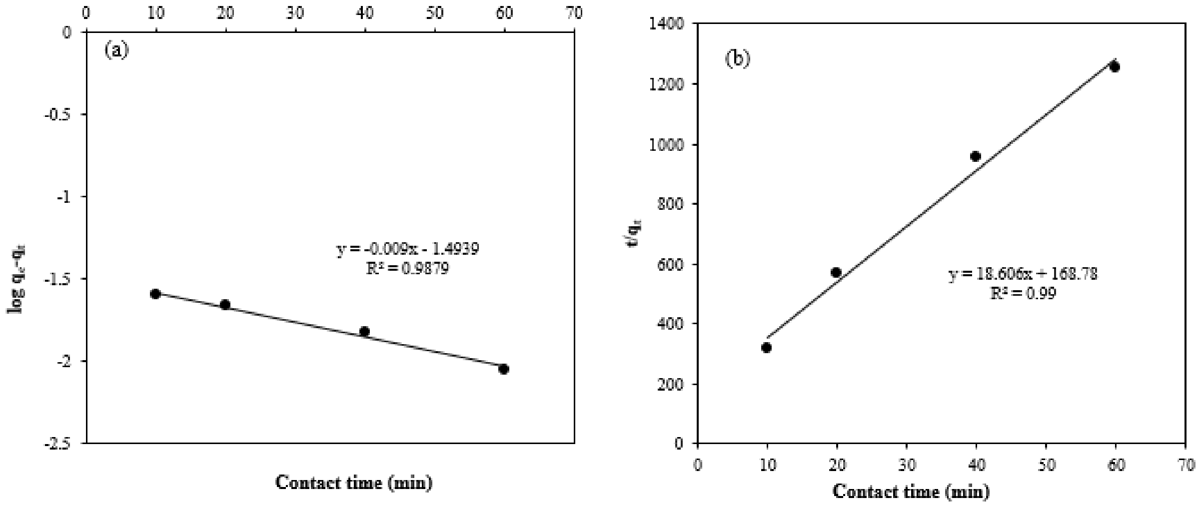

Figure 8. Graph of a) pseudo-first order b) pseudo-second order kinetic model for adsorption of PFOS.

Characterization of SA-β-CD hydrogel after PFOS adsorption experiment: FTIR analysis

According to Figure 9, the hydroxyl (OH) group exhibits a strong and broad stretching peak at 3420 cm^{-1}. A medium stretching peak for the C-H group is observed at 2931 cm^{-1}. The weak stretching peak at 1717 cm^{-1} is attributed to the C=O group. The sulfonate (S=O) group shows a medium and sharp stretching peak at 1220cm^{-1}.

Medium and sharp peaks for C-O stretching are observed at 1080 cm^{-1} and 1065 cm^{-1}. A weak stretching peak for the C-F group is identified at 1036 cm^{-1}. The C-O stretching functional group exhibited a weak peak at 950 cm^{-1}. A strong and sharp peak at 772 cm^{-1} corresponded to C-H bending [61]. The peaks at 3420 cm^{-1}, 1080 cm^{-1}, and 772 cm^{-1} shown on the spectrum for SA-β-CD hydrogel beads after adsorbing PFOS indicated the presence of β-CD, while the peak at 950 cm^{-1} signified SA. The peak at 1065 cm^{-1} corresponds to the C-O group formed between β-CD and epichlorohydrin. After the adsorption of PFOS, the peak for O-H stretching shifts slightly, and its intensity increased, making the peak stronger and sharper [62, 63]. Additionally, some bands observed in the spectrum of SA-β-CD hydrogel beads after PFOS adsorption were not present in the spectrum before adsorption, as in the medium and sharp bands for the S=O group at 1220 cm^{-1} and the medium band for the C-F group at 1036 cm^{-1}. The band at 1080 cm^{-1}, produced by the interaction of β-CD with epichlorohydrin, also remains evident [64].

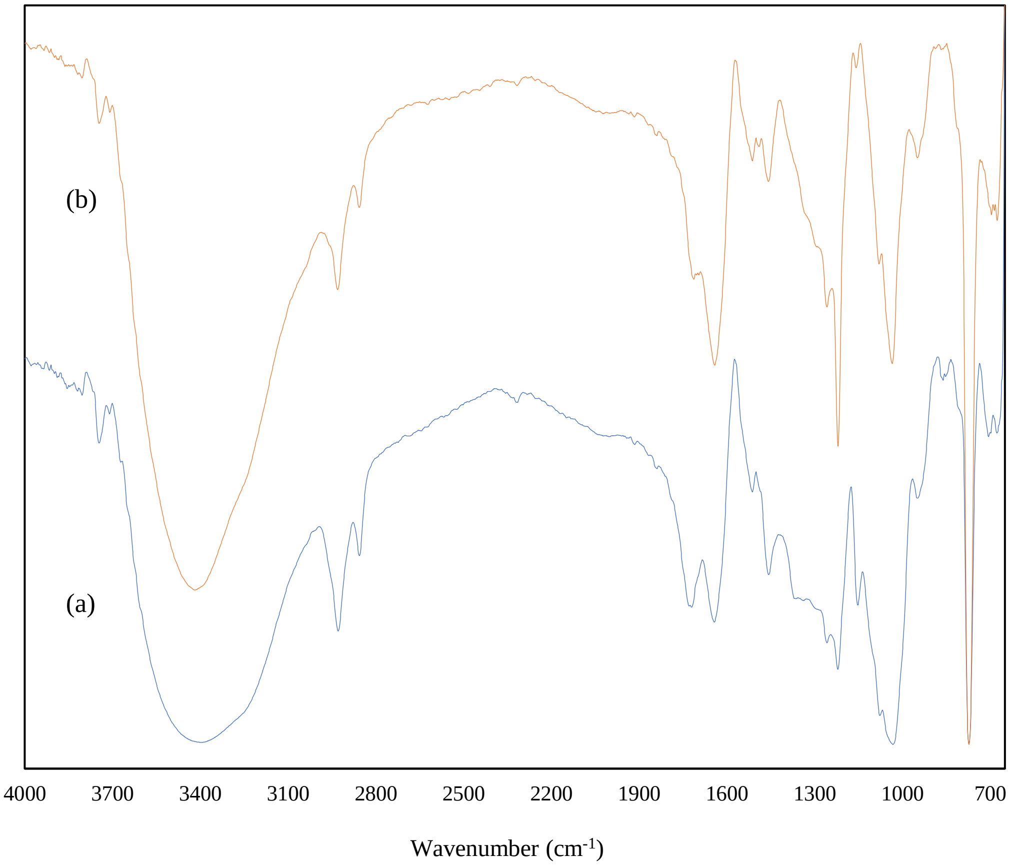

Figure 9. FTIR spectra of (a) SA-β-CD hydrogel (b) SA-β-CD hydrogel loaded PFOS.

Surface morphology

Due to the adherence of PFOS on the surface of the SA-β-CD hydrogel beads, the porosities of the SA-β-CD hydrogel beads after adsorption of PFOS were visibly minimized under different magnifications, as seen Figure 10 (e), (f), (g) and (h). It proved a successful adhesion of PFOS on the surface sites of SA-β-CD hydrogel beads, which were most likely via hydrophobic and electrostatic interactions. Aside from that, Figure 10 shows the surface of SA-β-CD hydrogel beads appearing rougher after the adsorption of PFOS compared to before the adsorption.

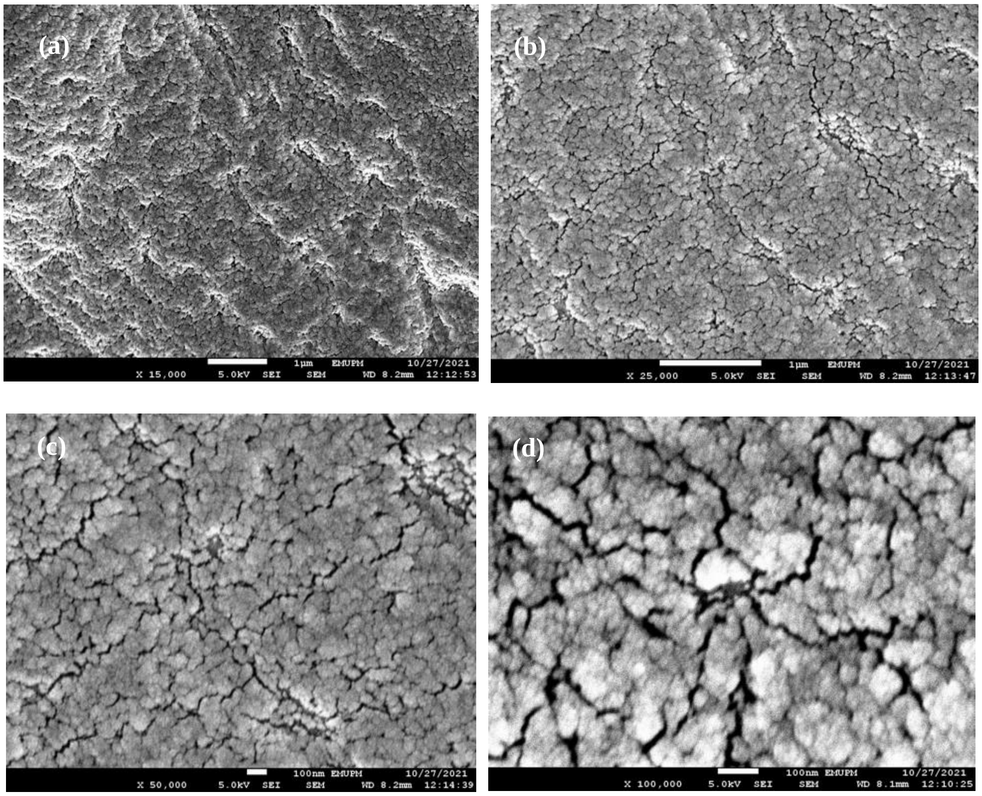

Figure 10. Surface morphologies of SA-β-CD hydrogel beads after adsorption of PFOS under magnifications of (a)15,000 (b) 25,000 (c) 50,000 and (d) 100,000.

Possible chemical interaction of PFOS and SA-β-CD hydrogel

The fluorocarbon part of PFOS holds hydrophobic, lipophilic, and nonpolar properties. In contrast, the other part of the PFOS containing the sulfonate group has hydrophilic and lipophilic properties which resulted in the molecule's addition of polarity. A strong hydrophobic effect on the chain of C-F of PFOS occurred when the PFOS was adsorbed onto the adsorbent of SA-β-CD hydrogel beads due to the hydrophobicity properties of β-CD on its structure. Hassan et al. stated that the hydrophobic interaction was the most prevalent mode of PFOS sorption when the fluorinated chain of PFOS interacted with the hydrophobic sites of the hydrogel. When the hydrophobic sites of β-cyclodextrin had promoted the hydrophobic effect, the removal efficiency and the adsorption capacity of PFOS were induced [60]. Furthermore, during such a penetration phenomenon, the electrostatic repulsions between the anionic nature of PFOS and the negatively charged SA-β-CD hydrogel surfaces can be overcome through hydrophobic interactions between fluorinated chains [64]. The adsorption phenomenon depends on the functional groups of the SA-β-CD and C-F chain length, which has been increased by the hydrophobic effect between PFOS and SA-β-CD hydrogel. [65-66]. On the other hand, sodium alginate and β-cyclodextrin also abundantly contain hydroxyl and carboxyl, influencing the adsorption efficiency of the PFOS on SA-β-CD hydrogel concerning electrostatic and hydrogen bonds interaction between them [67-68]. Hence, it has been proven that surface complexation and electrostatic interaction have been the reason for PFOS molecules to entrap to the surfaces of adsorbents [69]. The chemical interaction between SA-β-CD hydrogel adsorbent and PFOS offers a favourable interaction, including electrostatic, hydrogen bonding, and hydrophobic interactions for efficient removal. It is due to incorporating all constituents, including sodium alginate and β-cyclodextrin, into a single functionalised adsorbent that leads to substantial and strong chemical interaction between PFOS and SA-β-CD hydrogel adsorbent [70].

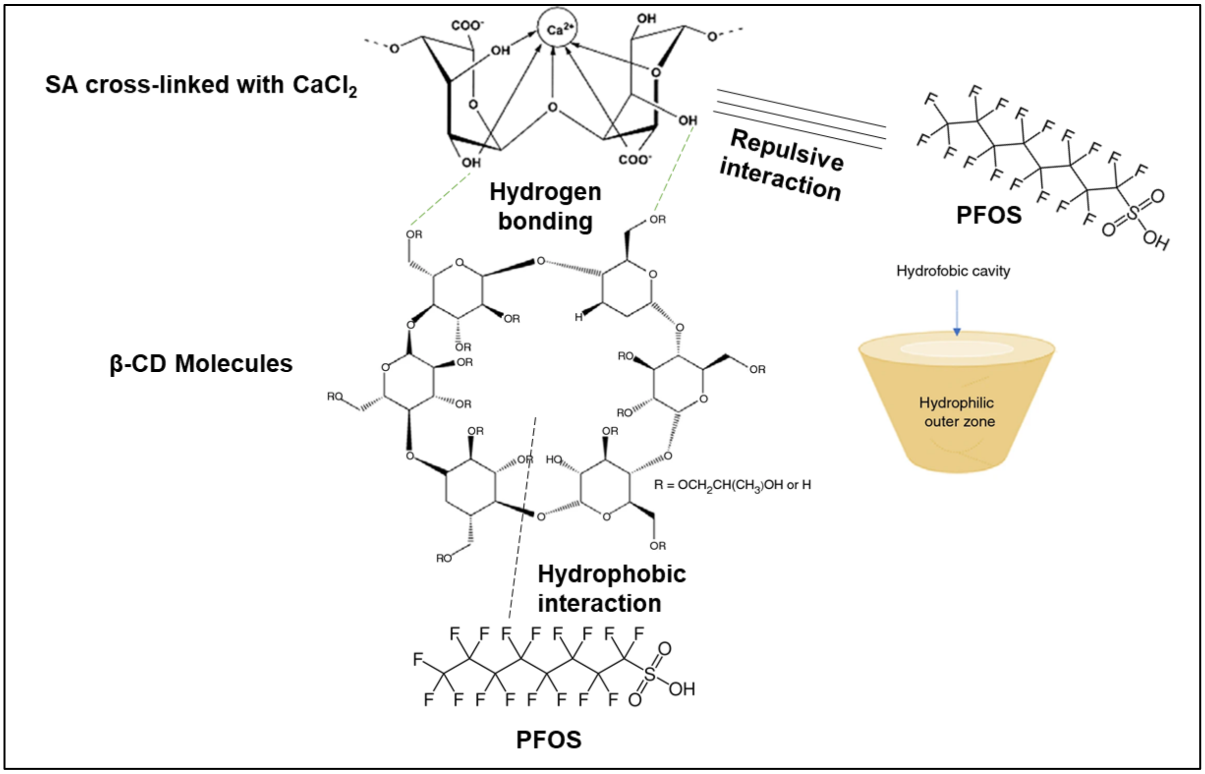

Figure 11. Possible interaction mechanism between PFOS with SA-β-CD hydrogel beads.

Conclusion

The SA-β-CD hydrogel has been substantially developed using a crosslinking immobilization reaction involving several biopolymers. This approach results in the formation of hydrogels with notable features such as great morphology, a high surface area, a stable structure, and excellent physical properties. The effectiveness of the production of the SA-β-CD hydrogel adsorbent was confirmed by FTIR spectroscopy. Based on the FTIR spectra, the peak band for O-H stretching slightly shifted, and its strength appeared to be enhanced, indicating that the SA-β-CD hydrogel beads had absorbed PFOS, causing the peak to become stronger and sharper. Besides, the rough surface of SA-β-CD hydrogel beads indicated that the PFOS had successfully adsorbed onto the surfaces which can be confirmed by using FESEM. Furthermore, the porosities of the SA-β-CD hydrogel beads seemed to decrease after the adsorption as fewer pores were seen on the surfaces than before the adsorption of PFOS was done. All the data obtained from the experiment using these parameters showed a matching hypothesis with the reference journals that studied the adsorption of PFOS. The findings show the optimum sorption at equilibrium conditions was attained through a batch adsorption experiment for PFOS by using 1280 mg dose of SA-β-CD hydrogels beads at 70°C, contact time of 30 minutes, a pH of 5.5, 10 mL of 10.0 ppm of solution, and 250 rpm stirring rate. In addition, the adsorption kinetic study showed that the pseudo-second-order model was chosen to describe the adsorption experiment of PFOS on the SA-β-CD hydrogel beads. However, the Langmuir adsorption isotherm study best fits the isotherm model with a higher R^2 value reported, explaining the adsorption of PFOS. Therefore, this work demonstrated the development of hydrogel as a successful supramolecular adsorbent that was able to remove PFOS at the highest percentage removal of 84.72 % and adsorption capacity of 0.0764 mg/g after incorporating β-CD to alginate properties when all the operational parameters were used.

Acknowledgements

The authors would like to convey their sincere appreciation to the Kurita Asia Research Grant (KARG) from Kurita Water and Environment Foundation (KWEF) (22PMY236) for their financial support for this research. The authors also acknowledge the Faculty of Science and Institute Bioscience (IBS), Universiti Putra

Malaysia for the facilities provided to carry out this project.

References

1. Xiao, F., Simcik, M. F., and Gulliver, J. S. (2013). Mechanisms for removal of perfluorooctane sulfonate (PFOS) and perfluorooctanoate (PFOA) from drinking water by conventional and enhanced coagulation. *Water Research,* 47(1): 49-56.
2. Franke, V., McCleaf, P., Lindegren, K., and Ahrens, L. (2019). Efficient removal of per- and polyfluoroalkyl substances (PFASs) in drinking water treatment: Nanofiltration combined with active carbon or anion exchange. *Environmental Science: Water Research and Technology,* 5(11): 1836-1843.
3. Wang, Y., and Zhu, H. (2014). Detection of PFOS and copper (II) ions based on complexation induced fluorescence quenching of porphyrin molecules. *Analytical Methods,* 6(7): 2379-2383.
4. Zhao, Y. G., Wong, C. K. C., and Wong, M. H. (2012). Environmental contamination, human exposure and body loadings of perfluorooctane sulfonate (PFOS), focusing on Asian countries. *Chemosphere,* 89(4): 355-368.
5. Buck, R. C., Franklin, J., Berger, U., Conder, J. M., Cousins, I. T., De Voogt, P., ... and van Leeuwen, S. P. (2011). Perfluoroalkyl and polyfluoroalkyl substances in the environment: terminology, classification, and origins. *Integrated Environmental Assessment and Management, 7*(4): 513-541.
6. Li, X., Chen, S., Quan, X., and Zhang, Y. (2011). Enhanced adsorption of PFOA and PFOS on multiwalled carbon nanotubes under electrochemical assistance. *Environmental Science and Technology,* 45(19): 8498-8505.
7. Yan, T., Chen, H., Jiang, F., and Wang, X. (2014). Adsorption of perfluorooctane sulfonate and perfluorooctanoic acid on magnetic mesoporous carbon nitride. *Journal of Chemical & Engineering Data,* 59(2): 508-515.
8. Van Tran, V., Park, D., and Lee, Y. C. (2018). Hydrogel applications for adsorption of contaminants in water and wastewater treatment. *Environmental Science and Pollution Research,* 25(25): 24569-24599.
9. Alves, A. V., Tsianou, M., and Alexandridis, P. (2020). Fluorinated surfactant adsorption on mineral surfaces: Implications for PFAS fate and transport in the environment. *Surfaces,* 3(4): 516-566.
10. Lee, P., and Rogers, M. A. (2012). Effect of calcium source and exposure-time on basic caviar spherification using sodium alginate. *International Journal of Gastronomy and Food Science,* 1(2): 96-100.
11. Puscaselu, R. G., Lobiuc, A., Dimian, M., and Covasa, M. (2020). Alginate: from food industry to biomedical applications and management of metabolic disorders. *Polymers,* 12(10): 2417.
12. Sánchez-Fernández, J., Presbítero-Espinosa, G., Peña-Parás, L., Pizaña, E. I. R., Galván, K. P. V., Vopalensky, M., Kumpová, I., and Elizalde-Herrera, L. E. (2021). Characterization of sodium alginate hydrogels reinforced with nanoparticles of hydroxyapatite for biomedical applications. *Polymers,* 13(17): 2927.
13. Gidwani, B., and Vyas, A. (2014). Synthesis, characterization and application of epichlorohydrin-β-cyclodextrin polymer. *Colloids and Surfaces B: Biointerfaces,* 114: 130-137.
14. Păduraru, D. N., Niculescu, A. G., Bolocan, A., Andronic, O., Grumezescu, A. M., and Bîrlă, R. (2022). An updated overview of cyclodextrin-based drug delivery systems for cancer therapy. *Pharmaceutics,* 14(8):1748.
15. Yadav, V. R., Suresh, S., Devi, K., and Yadav, S. (2009). Effect of cyclodextrin complexation of curcumin on its solubility and antiangiogenic and anti-inflammatory activity in rat colitis model. *AAPS PharmSciTech,* 10(3): 752-62.
16. Qin, X., Bai, L., Tan, Y., Li, L., Song, F., and Wang, Y. (2019). β-Cyclodextrin-crosslinked polymeric adsorbent for simultaneous removal and stepwise recovery of organic dyes and heavy metal ions: Fabrication, performance and mechanisms. *Chemical Engineering Journal,* 372: 1007-1018.
17. Belenguer-Sapiña, C., Pellicer-Castell, E., Mauri-Aucejo, A. R., Simó-Alfonso, E. F., and Amorós, P. (2020). Cyclodextrins as a key piece in nanostructured materials: Quantitation and remediation of pollutants. *Nanomaterials,* 11(1): 7.
18. Yadav, S., Asthana, A., Singh, A. K., Chakraborty, R., Vidya, S. S., Susan, M. A. B. H., and Carabineiro, S. A. C. (2021). Adsorption of cationic dyes, drugs and metal from aqueous

solutions using a polymer composite of magnetic/β-cyclodextrin/activated charcoal/Na alginate: Isotherm, kinetics and regeneration studies. Journal of Hazardous Materials, 409(8):124840.

19. Liu, Z., Sun, Y., Xu, X., Qu, J., and Qu, B. (2020). Adsorption of Hg(II) in an aqueous solution by activated carbon prepared from rice husk using KOH activation. *ACS Omega*, 5(45): 29231-29242.
20. Chen, A. H., Liu, S. C., Chen, C. Y., and Chen, C. Y. (2008). Comparative adsorption of Cu(II), Zn(II), and Pb(II) ions in aqueous solution on the crosslinked chitosan with epichlorohydrin. *Journal of Hazardous Materials*, 154(1–3): 184-191.
21. Melo, B. C., Paulino, F. A. A., Cardoso, V. A., Pereira, A. G. B., Fajardo, A. R., and Rodrigues, F. H. A. (2018). Cellulose nanowhiskers improve the methylene blue adsorption capacity of chitosan-g-poly(acrylic acid) hydrogel. *Carbohydrate Polymers*, 181: 358-367.
22. Zulfiqar, M., Lee, S. Y., Mafize, A. A., Kahar, N. A. M. A., Johari, K., and Rabat, N. E. (2020). Efficient removal of Pb (II) from aqueous solutions by using oil palm bio-waste/MWCNTs reinforced PVA hydrogel composites: kinetic, isotherm and thermodynamic modeling. *Polymers*, 12(2): 430.
23. Elanchezhiyan, S., Muthu Prabhu, S., Han, J., Kim, Y. M., Yoon, Y., and Park, C. M. (2020). Synthesis and characterization of novel magnetic Zr-$MnFe_2O_4$@rGO nanohybrid for efficient removal of PFOA and PFOS from aqueous solutions. *Applied Surface Science*, 528:146579.
24. Wang, B., Gao, B., Zimmerman, A. R., and Lee, X. (2018). Impregnation of multiwall carbon nanotubes in alginate beads dramatically enhances their adsorptive ability to aqueous methylene blue. *Chemical Engineering Research and Design*, 133: 235-242.
25. Badruddoza, A. Z. M., Bhattarai, B., and Suri, R. P. S. (2017). Environmentally friendly β-cyclodextrin–ionic liquid polyurethane-modified magnetic sorbent for the removal of PFOA, PFOS, and Cr(VI) from water. *ACS Sustainable Chemistry & Engineering*, 5(10): 9223-9232.
26. Rahimi, Z., Zinatizadeh, A. A., Zinadini, S., and van Loosdrecht, M. C. M. (2020). β-cyclodextrin functionalized MWCNTs as a promising antifouling agent in fabrication of composite nanofiltration membranes. *Separation and Purification Technology*, 247(10): 116979.
27. Ragavan, K., and Rastogi, N. K. (2017). β-Cyclodextrin capped graphene-magnetite nanocomposite for selective adsorption of Bisphenol-A. *Carbohydrate Polymers*, 168: 129-137.
28. Qian, Z. J., Zhang, J., Xu, W. R., and Zhang, Y. C. (2022). Development of active packaging films based on liquefied shrimp shell chitin and polyvinyl alcohol containing β-cyclodextrin/cinnamaldehyde inclusion. *International Journal of Biological Macromolecules*, 214(3): 67-76.
29. Verma, A., Thakur, S., Mamba, G., Prateek, Gupta, R. K., Thakur, P., and Thakur, V. K. (2020). Graphite modified sodium alginate hydrogel composite for efficient removal of malachite green dye. *International Journal of Biological Macromolecules*, 148: 1130-1139.
30. Zhijiang, C., Cong, Z., Ping, X., Jie, G., and Kongyin, Z. (2018). Calcium alginate-coated electrospun polyhydroxybutyrate/carbon nanotubes composite nanofibers as nanofiltration membrane for dye removal. *Journal of Materials Science*, 53(20): 14801-14820.
31. Thakur, S., and Arotiba, O. (2018). Synthesis, characterization and adsorption studies of an acrylic acid-grafted sodium alginate-based TiO_2 hydrogel nanocomposite. *Adsorption Science and Technology*, 36(1–2): 458-477.
32. Wu, Y., Qi, H., Shi, C., Ma, R., Liu, S., and Huang, Z. (2017). Preparation and adsorption behaviors of sodium alginate-based adsorbent-immobilized β-cyclodextrin and graphene oxide. *RSC Advances*, 7(50): 31549-31557.
33. Darini, A., Eslaminejad, T., Nematollahi Mahani, S. N., and Ansari, M. (2019). Magnetogel nanospheres composed of cisplatin-loaded alginate/β-cyclodextrinas controlled release drug delivery. *Advanced Pharmaceutical Bulletin*, 9(4): 571-577.
34. Godiya, C. B., Xiao, Y., and Lu, X. (2020). Amine functionalized sodium alginate hydrogel for efficient and rapid removal of methyl blue in water. *International Journal of Biological Macromolecules*, 144: 671-681.
35. Yang, J.-S, Han, S.-Y, Yang, L., and Zheng, H.-C. (2014). Synthesis of beta-cyclodextrin-grafted-

alginate and its application for removing methylene blue from water solution. *Journal of Chemical Technology & Biotechnology,* 91(3): 618-623.

36. Shen, Y., Niu, L., Yu, Z., Wang, M., Shang, Z., and Yang, Y. (2018). Sodium alginate-grafted β-cyclodextrins as a matrix for immobilized Arthrobacter simplex for cortisone acetate biotransfromation. *Applied Surface Science,* 444: 42-47.
37. Shen, L., Jin, Z., Wang, D., Wang, Y., and Lu, Y. (2018). Enhance wastewater biological treatment through the bacteria induced graphene oxide hydrogel. *Chemosphere,* 190: 201-210.
38. Cataldo, S., Muratore, N., Orecchio, S., and Pettignano, A. (2015). Enhancement of adsorption ability of calcium alginate gel beads towards Pd(II) ion. A kinetic and equilibrium study on hybrid Laponite and Montmorillonite–alginate gel beads. *Applied Clay Science,* 118: 162-170.
39. Kurwadkar, S., Dane, J., Kanel, S. R., Nadagouda, M. N., Cawdrey, R. W., Ambade, B., Struckhoff, G. C., & Wilkin, R. T. (2022). Per- and polyfluoroalkyl substances in water and wastewater: A critical review of their global occurrence and distribution. *Science of the Total Environment,* 809: 151003.
40. Barton, K., Starling, A. P., Higgins, C. P., McDonough, C. A., Calafat, A. M., and Adgate, J. L. (2020). Sociodemographic and behavioral determinants of serum concentrations of per- and polyfluoroalkyl substances in a community highly exposed to aqueous film-forming foam contaminants in drinking water. *International Journal of Hygiene and Environmental Health,* 223(1): 256-266.
41. Asadi, S., Eris, S., and Azizian, S. (2018). Alginate-based hydrogel beads as a biocompatible and efficient adsorbent for dye removal from aqueous solutions. *ACS Omega,* 3(11): 15140-15148.
42. Deng, S., Zhang, Q., Nie, Y., Wei, H., Wang, B., Huang, J., … Xing, B. (2012). Sorption mechanisms of perfluorinated compounds on carbon nanotubes. *Environmental Pollution,* 168: 138-144.
43. Taka, A. L., Fosso-Kankeu, E., Pillay, K., and Mbianda, X. Y. (2018). Removal of cobalt and lead ions from wastewater samples using an insoluble nanosponge biopolymer composite: adsorption isotherm, kinetic, thermodynamic, and regeneration studies. *Environmental Science and Pollution Research,* 25(22), 21752-21767.
44. Guo, W., Huo, S., Feng, J., & Lu, X. (2017). Adsorption of perfluorooctane sulfonate (PFOS) on corn straw-derived biochar prepared at different pyrolytic temperatures. *Journal of the Taiwan Institute of Chemical Engineers,* 78: 265-271.
45. Wang, F., & Shih, K. (2011). Adsorption of perfluorooctanesulfonate (PFOS) and perfluorooctanoate (PFOA) on alumina: Influence of solution pH and cations. *Water Research,* 45(9): 2925-2930.
46. Guo, W., Huo, S., Feng, J., and Lu, X. (2017). Adsorption of perfluorooctane sulfonate (PFOS) on corn straw-derived biochar prepared at different pyrolytic temperatures. *Journal of the Taiwan Institute of Chemical Engineers,* 78: 265-271.
47. Yan, T., Chen, H., Jiang, F., and Wang, X. (2014). Adsorption of perfluorooctane sulfonate and perfluorooctanoic acid on magnetic mesoporous carbon nitride. *Journal of Chemical and Engineering Data,* 59(2): 508-515.
48. Gagliano, E., Sgroi, M., Falciglia, P. P., Vagliasindi, F. G. A., and Roccaro, P. (2020). Removal of poly- and perfluoroalkyl substances (PFAS) from water by adsorption: Role of PFAS chain length, effect of organic matter and challenges in adsorbent regeneration. *Water Research,* 171: 115381.
49. Khan, S. A., Siddiqui, M. F., and Khan, T. A. (2020). Synthesis of poly(methacrylic acid)/montmorillonite hydrogel nanocomposite for efficient adsorption of amoxicillin and diclofenac from aqueous environment: kinetic, isotherm, reusability, and thermodynamic investigations. *ACS Omega,* 2020: 361.
50. Bei, Y., Deng, S., Du, Z., Wang, B., Huang, J., and Yu, G. (2014). Adsorption of perfluorooctane sulfonate on carbon nanotubes: Influence of pH and competitive ions. *Water Science and Technology,* 69(7): 1489-1495.
51. Gutierrez, A. M., Frazar, E. M., Klaus, V., Paul, P., and Hilt, J. Z. (2021). Hydrogels and hydrogel nanocomposites: Enhancing healthcare through human and environmental treatment. *Advanced Healthcare Materials,* 11(7): 2101820.

52. Huang, Z., Liu, S., Zhang, B., and Wu, Q. (2014). Preparation and swelling behavior of a novel self-assembled β-cyclodextrin/acrylic acid/sodium alginate hydrogel. *Carbohydrate Polymers,* 113: 430-437.
53. Liu, Z., Sun, Y., Xu, X., Qu, J., and Qu, B. (2020). Adsorption of Hg(II) in an aqueous solution by activated carbon prepared from rice husk using KOH activation. *ACS Omega,* 5(45): 29231-29242.
54. Al-Harby, N. F., Albahly, E. F., and Mohamed, N. A. (2021). Kinetics, isotherm and thermodynamic studies for efficient adsorption of congo red dye from aqueous solution onto novel cyanoguanidine-modified chitosan adsorbent. *Polymers,* 13(24): 4446.
55. Elanchezhiyan, S., Muthu Prabhu, S., Han, J., Kim, Y. M., Yoon, Y., and Park, C. M. (2020). Synthesis and characterization of novel magnetic Zr-$MnFe_2O_4$@rGO nanohybrid for efficient removal of PFOA and PFOS from aqueous solutions. *Applied Surface Science,* 528: 146579.
56. Hasani, N., Selimi, T., Mele, A., Thaçi, V., Halili, J., Berisha, A., and Sadiku, M. (2022). Theoretical, equilibrium, kinetics and thermodynamic investigations of methylene blue adsorption onto lignite coal. *Molecules,* 27(6): 1856.
57. Sahara, T., Wongsawaeng, D., Ngaosuwan, K., Kiatkittipong, W., Hosemann, P., and Assabumrungrat, S. (2023). Highly effective removal of perfluorooctanoic acid (PFOA) in water with DBD-plasma-enhanced rice husks. *Scientific Reports,* 13(1): 40197.
58. Khamizov, R. Kh. (2020). A pseudo-second order kinetic equation for sorption processes. *Russian Journal of Physical Chemistry* A, 94(1): 171-176.
59. León, G., Hidalgo, A., Martínez, A., Guzmán, M. A., and Miguel, B. (2023). Methylparaben adsorption onto activated carbon and activated olive stones: comparative analysis of efficiency, equilibrium, kinetics and effect of graphene-based nanomaterials addition. *Applied Sciences,* 13(16): 9147.
60. Hassan, M., Liu, Y., Naidu, R., Du, J., and Qi, F. (2020). Adsorption of perfluorooctane sulfonate (PFOS) onto metal oxides modified biochar. *Environmental Technology and Innovation,* 19: 100816.
61. Chen, W., Zhang, X., Mamadiev, M., and Wang, Z. (2017). Sorption of perfluorooctane sulfonate and perfluorooctanoate on polyacrylonitrile fiber-derived activated carbon fibers: In comparison with activated carbon. *RSC Advances,* 7(2): 927-938.
62. Shen, Y., Niu, L., Yu, Z., Wang, M., Shang, Z., and Yang, Y. (2018). Sodium alginate-grafted β-cyclodextrins as a matrix for immobilized Arthrobacter simplex for cortisone acetate biotransfromation. *Applied Surface Science,* 444: 42-47.
63. Niu, B., Yang, S., Li, Y., Zang, K., Sun, C., Yu, M., … Zheng, Y. (2020). Regenerable magnetic carbonized Calotropis gigantea fiber for hydrophobic-driven fast removal of perfluoroalkyl pollutants. *Cellulose,* 27(10): 5893-5905.
64. Zaggia, A., Conte, L., Falletti, L., Fant, M., Chiorboli, A. (2016). Use of strong anion exchange resins for the removal of perfluoroalkylated substances from contaminated drinking water in batch and continuous pilot plants. *Water Research,* 91: 137-146.
65. McCleaf, P., Englund, S., Oestlund, A., Lindegren, K., Wiberg, K., Ahrens, L. (2017). Removal efficiency of multiple poly- and perfluoroalkyl substances (PFASs) in drinking water using granular activated carbon (GAC) and anion exchange (AE) column tests. *Water Research,* 120: 77e87.
66. Rahman, M. F., Peldszus, S., Anderson, W. B., (2014). Behaviour and fate of per- fluoroalkyl and polyfluoroalkyl substances (PFASs) in drinking water treatment: a review. *Water Research,* 50: 318-340.
67. Appleman, T. D., Higgins, C. P., Quin~ones, O., Vanderford, B. J., Kolstad, C., Zeigler- Holady, J. C., Dickenson, E. R. V. (2014). Treatment of poly- and perfluoroalkyl substances in U.S. full-scale water treatment systems. *Water Research,* 51: 246-255.
68. Xiao, F., Zhang, X., Penn, L., Gulliver, J. S. and Simcik, M. F. (2011). Effects of monovalent cations on the competitive adsorption of perfluoroalkyl acids by kaolinite: experimental studies and modeling. *Environmental Science Technology,* 45: 10028-10035.
69. Campos-Pereira, H., Kleja, D. B., Sjöstedt, C., Ahrens, L., Klysubun, W., and Gustafsson, J. P. (2020). The adsorption of per- and polyfluoroalkyl substances (PFASs) onto ferrihydrite is governed

by surface charge. *Environmental Science & Technology*, 54(24): 15722-15730.

70. Zhan, W., Gao, L., Fu, X., Siyal, S. H., Sui, G., and Yang, X. (2019). Green synthesis of amino-functionalized carbon nanotube-graphene hybrid aerogels for high performance heavy metal ions removal. *Applied Surface Science*, 467-468: 1122-1133.